Research Article | Vol. 25, No. 19 | 18 Sep 2017 | OPTICS EXPRESS 23502
Optics EXPRESS

High harmonic generation from axial chiral molecules

DIAN WANG,[1] XIAOSONG ZHU, [1,*] XI LIU,[1] LIANG LI,[1] XIAOFAN ZHANG,[1] PENGFEI LAN,[1] PEIXIANG LU[1,2,3]

[1]*Wuhan National Laboratory for Optoelectronics and School of Physics, Huazhong University of Science and Technology, Wuhan 430074, China*
[2]*Laboratory of Optical Information Technology, Wuhan Institute of Technology, Wuhan 430205, China*
[3]*lupeixiang@hust.edu.cn*
[*]*zhuxiaosong@hust.edu.cn*

Abstract: Axial chiral molecules, whose stereogenic element is an axis rather than a chiral center, have attracted widespread interest due to their important application, such as asymmetric synthesis and chirality transfer. We investigate high harmonic generation from axial chiral molecules with bichromatic counterrotating circularly polarized laser fields. High harmonic generation from three typical molecules: (S_a)-3-chloropropa-1,2-dien-1-ol, propadiene, and (R_a)-2,3-pentadiene is simulated with time-dependent density-functional theory and strong field approximation. We found that harmonic spectra for 3D oriented axial chiral molecules exhibit obvious circular dichroism. However, the circular dichroism of High harmonic generation from an achiral molecule is much trivial. Moreover, the dichroism of high harmonic generation still exists when axial chiral molecules are 1D oriented,such as (S_a) -3-chloropropa-1,2-dien-1-ol. For a special form of axial chiral molecules with the formula abC=C=Cab (a, b are different substituents), like (R_a)-2,3-pentadiene, the dichroism discriminations disappear when the molecules are only in 1D orientation. The circular dichroism of high harmonic generation from axial chiral molecules is well explained by the trajectory analysis based on the semiclassical three-step mechanism.

OCIS codes: (160.1585) Chiral media; (190.4160) Multiharmonic generation; (020.2649) Strong field laser physics.

References and links

1. N. Berova, P. Polavarapu, K. Nakanishi, and R. Woody, *Comprehensive Chiroptical Spectroscopy: Instrumentation, Methodologies, and Theoretical Simulations. Vol. 1* (John Wiley & Sons, Inc, 2012).
2. D. Patterson, M. Schnell, and J. M. Doyle, "Enantiomer-specific detection of chiral molecules via microwave spectroscopy," Nature **497**, 475–477 (2013).
3. I. Dreissigacker and M. Lein, "Photoelectron circular dichroism of chiral molecules studied with a continuum-state-corrected strong-field approximation," Phys. Rev. A **89**, 053406 (2014).
4. N. Böwering, T. Lischke, B. Schmidtke, N. Müller, T. Khalil, and U. Heinzmann, "Asymmetry in photoelectron emission from chiral molecules induced by circularly polarized light," Phys. Rev. Lett. **86**, 1187–1190 (2001).
5. C. Lux, M. Wollenhaupt, T. Bolze, Q. Liang, J. Köhler, C. Sarpe, and T. Baumert, "Circular dichroism in the photoelectron angular distributions of camphor and fenchone from multiphoton ionization with femtosecond laser pulses," Angew. Chem. Int. Ed. **51**, 5001–5005 (2012).
6. A. Ferré, C. Handschin, M. Dumergue, F. Burgy, A. Comby, D. Descamps, B. Fabre, G. A. Garcia, R. Géneaux, L. Merceron, Others, E. Mével, L. Nahon, S. Petit, B. Pons, D. Staedter, S. Weber, T. Ruchon, V. Blanchet, and Y. Mairesse, "A table-top ultrashort light source in the extreme ultraviolet for circular dichroism experiments," Nat. Photon. **9**, 93–98 (2015).
7. K. Liu, K. Renziehausen, and I. Barth, "Producing spin-polarized photoelectrons by using the momentum gate in strong-field ionization experiments," Phys. Rev. A **95**, 063410 (2017).
8. R. Cireasa, A. E. Boguslavskiy, B. Pons, M. C. H. Wong, D. Descamps, S. Petit, H. Ruf, N. Thiré, A. Ferré, J. Suarez, J. Higuet, B. E. Schmidt, A. F. Alharbi, F. Légaré, V. Blanchet, B. Fabre, S. Patchkovskii, O. Smirnova, Y. Mairesse, and V. R. Bhardwaj, "Probing molecular chirality on a sub-femtosecond timescale," Nat. Phys. **11**, 654–658 (2015).
9. O. Smirnova, Y. Mairesse, and S. Patchkovskii, "Opportunities for chiral discrimination using high harmonic generation in tailored laser fields," J. Phys. B: At. Mol. Opt. Phys. **48**, 234005 (2015).
10. X. Zhu, X. Liu, P. Lan, D. Wang, Q. Zhang, W. Li, and P. Lu, "Anomalous circular dichroism in high harmonic generation of stereoisomers with two chiral centers," Opt. Express **24**, 24824–24835 (2016).
11. F. Krausz and M. Ivanov, "Attosecond physics," Rev. Mod. Phys. **81**, 163–234 (2009).

#303845 https://doi.org/10.1364/OE.25.023502
Journal © 2017 Received 2 Aug 2017; revised 9 Sep 2017; accepted 11 Sep 2017; published 15 Sep 2017

Optics EXPRESS

12. E. J. Takahashi, P. Lan, O. D. Mücke, Y. Nabekawa, and K. Midorikawa, "Infrared two-color multicycle laser field synthesis for generating an intense attosecond pulse," Phys. Rev. Lett. **104**, 233901 (2010).
13. L. Li, Z. Wang, F. Li, and H. Long, "Efficient generation of highly elliptically polarized attosecond pulses," Opt. Quantum Electron **49**, 73 (2017).
14. H. Yuan, L. He, F. Wang, B. Wang, W. Liu, and Z. Hong, "Generation of isolated attosecond pulses in a multi-cycle inhomogeneous two-color field without cep stabilization," Opt Quantum Electron **49**, 214 (2017).
15. P. M. Kraus, B. Mignolet, D. Baykusheva, A. Rupenyan, L. Horný, E. F. Penka, G. Grassi, O. I. Tolstikhin, J. Schneider, F. Jensen, L. B. Madsen, A. D. Bandrauk, F. Remacle, and H. J. Wörner, "Measurement and laser control of attosecond charge migration in ionized iodoacetylene," Science **350**, 790–795 (2015).
16. X. Liu, P. Li, X. Zhu, P. Lan, Q. Zhang, and P. Lu, "Probing the $\pi - \pi^*$ transitions in conjugated compounds with an infrared femtosecond laser," Phys. Rev. A **95**, 033421 (2017).
17. O. Smirnova, Y. Mairesse, S. Patchkovskii, N. Dudovich, D. Villeneuve, P. Corkum, and M. Y. Ivanov, "High harmonic interferometry of multi-electron dynamics in molecules," Nature **460**, 972–977 (2009).
18. P. Lan, M. Ruhmann, L. He, C. Zhai, F. Wang, X. Zhu, Q. Zhang, Y. Zhou, M. Li, M. Lein, and P. Lu, "Attosecond probing of nuclear dynamics with trajectory-resolved high-harmonic spectroscopy," Phys. Rev. Lett. **119**, 033201 (2017).
19. X. Liu, X. Zhu, P. Lan, X. Zhang, D. Wang, Q. Zhang, and P. Lu, "Time-dependent population imaging for high-order-harmonic generation in solids," Phys. Rev. A **95**, 063419 (2017).
20. Z. Wang, K. Liu, P. Lan, and P. Lu, "Control of electron localization in highly excited states with two ultraviolet laser pulses," J. Phys. B: At. Mol. Opt. Phys. **48**, 015601 (2014).
21. M. Qin and X. Zhu, "Molecular orbital imaging for partially aligned molecules," Opt. Laser Technol. **87**, 79–86 (2017).
22. C. Zhai, X. Zhu, P. Lan, F. Wang, L. He, W. Shi, Y. Li, M. Li, Q. Zhang, and P. Lu, "Diffractive molecular-orbital tomography," Phys. Rev. A **95**, 033420 (2017).
23. J. Itatani, J. Levesque, D. Zeidler, H. Niikura, H. Pépin, J. C. Kieffer, P. B. Corkum, and D. M. Villeneuve, "Tomographic imaging of molecular orbitals," Nature **432**, 867–871 (2004).
24. P. B. Corkum and F. Krausz, "Attosecond science," Nat. Phys. **3**, 381–387 (2007).
25. P. B. Corkum, "Plasma perspective on strong field multiphoton ionization," Phys. Rev. Lett. **71**, 1994–1997 (1993).
26. M. C. Kozlowski, B. J. Morgan, and E. C. Linton, "Total synthesis of chiral biaryl natural products by asymmetric biaryl coupling," Chem. Soc. Rev. **38**, 3193–3207 (2009).
27. A. Hoffmann-Röder and N. Krause, "Synthesis and properties of allenic natural products and pharmaceuticals," Angew. Chem. Int. Ed. **43**, 1196–1216 (2004).
28. R. Noyori and H. Takaya, "Binap: an efficient chiral element for asymmetric catalysis," Acc. Chem. Res. **23**, 345–350 (1990).
29. Y. Chen, S. Yekta, and A. K. Yudin, "Modified BINOL ligands in asymmetric catalysis," Chem. Rev. **103**, 3155–3212 (2003).
30. D. Campolo, S. Gastaldi, C. Roussel, M. P. Bertrand, and M. Nechab, "Axial-to-central chirality transfer in cyclization processes," Chem. Soc. Rev. **42**, 8434–8466 (2013).
31. E. Runge and E. K. U. Gross, "Density-functional theory for time-dependent systems," Phys. Rev. Lett. **52**, 997–1000 (1984).
32. N. Tancogne-Dejean, O. D. Mucke, F. X. Kartner, and A. Rubio, "Impact of the electronic band structure in high-harmonic generation spectra of solids," Phys. Rev. Lett. **118**, 087403 (2017).
33. X. Liu, X. Zhu, L. Li, Y. Li, Q. Zhang, P. Lan, and P. Lu, "Selection rules of high-order-harmonic generation: Symmetries of molecules and laser fields," Phys. Rev. A **94**, 033410 (2016).
34. C. Hartwigsen, S. Goedecker, and J. Hutter, "Relativistic separable dual-space gaussian pseudopotentials from h to rn," Phys. Rev. B **58**, 3641–3662 (1998).
35. J. P. Perdew, K. Burke, and M. Ernzerhof, "Generalized gradient approximation made simple," Phys. Rev. Lett. **77**, 3865–3868 (1996).
36. P. Hohenberg and W. Kohn, "Inhomogeneous electron gas," Phys. Rev. **136**, B864–B871 (1964).
37. W. Kohn and L. J. Sham, "Self-consistent equations including exchange and correlation effects," Phys. Rev. **140**, A1133–A1138 (1965).
38. A. Castro, M. A. L. Marques, and A. Rubio, "Propagators for the time-dependent kohn–sham equations," J. Chem. Phys. **121**, 3425–3433 (2004).
39. M. A. L. Marques, A. Castro, G. F. Bertsch, and A. Rubio, "octopus: a first-principles tool for excited electron–ion dynamics," Comput. Phys. Commun. **151**, 60–78 (2003).
40. M. Lewenstein, P. Balcou, M. Y. Ivanov, A. L'Huillier, and P. B. Corkum, "Theory of high-harmonic generation by low-frequency laser fields," Phys. Rev. A **49**, 2117–2132 (1994).
41. M. J. Frisch, G. W. Trucks, H. B. Schlegel, G. E. Scuseria, M. A. Robb, J. R. Cheeseman, G. Scalmani, V. Barone, B. Mennucci, G. A. Petersson, H. Nakatsuji, M. Caricato, X. Li, H. P. Hratchian, A. F. Izmaylov, J. Bloino, G. Zheng, J. L. Sonnenberg, M. Hada, M. Ehara, K. Toyota, R. Fukuda, J. Hasegawa, M. Ishida, T. Nakajima, Y. Honda, O. Kitao, H. Nakai, T. Vreven, J. A. Montgomery, Jr., J. E. Peralta, F. Ogliaro, M. Bearpark, J. J. Heyd, E. Brothers, K. N. Kudin, V. N. Staroverov, R. Kobayashi, J. Normand, K. Raghavachari, A. Rendell, J. C. Burant, S. S. Iyengar, J. Tomasi, M. Cossi, N. Rega, J. M. Millam, M. Klene, J. E. Knox, J. B. Cross, V. Bakken, C. Adamo, J. Jaramillo,

Optics EXPRESS

R. Gomperts, R. E. Stratmann, O. Yazyev, A. J. Austin, R. Cammi, C. Pomelli, J. W. Ochterski, R. L. Martin, K. Morokuma, V. G. Zakrzewski, G. A. Voth, P. Salvador, J. J. Dannenberg, S. Dapprich, A. D. Daniels, . Farkas, J. B. Foresman, J. V. Ortiz, J. Cioslowski, and D. J. Fox, "Gaussian 09 Revision D.1," Gaussian Inc. Wallingford CT 2009.
42. B. K. McFarland, J. P. Farrell, P. H. Bucksbaum, and M. Gühr, "High harmonic generation from multiple orbitals in N_2," Science **322**, 1232–1235 (2008).
43. M. He, Y. Li, Y. Zhou, M. Li, and P. Lu, "Temporal and spatial manipulation of the recolliding wave packet in strong-field photoelectron holography," Phys. Rev. A **93**, 033406 (2016).
44. X. Ma, M. Li, Y. Zhou, and P. Lu, "Nonsequential double ionization of Xe by mid-infrared laser pulses," Opt. Quantum Electron **49**, 170 (2017).
45. V. V. Strelkov, A. A. Gonoskov, I. A. Gonoskov, and M. Y. Ryabikin, "Origin for ellipticity of high-order harmonics generated in atomic gases and the sublaser-cycle evolution of harmonic polarization," Phys. Rev. Lett. **107**, 043902 (2011).
46. X. Zhu, X. Liu, Y. Li, M. Qin, Q. Zhang, P. Lan, and P. Lu, "Molecular high-order-harmonic generation due to the recollision mechanism by a circularly polarized laser pulse," Phys. Rev. A **91**, 043418 (2015).
47. O. Kfir, P. Grychtol, E. Turgut, R. Knut, D. Zusin, D. Popmintchev, T. Popmintchev, H. Nembach, J. M. Shaw, A. Fleischer, H. Kapteyn, M. Murnane, and O. Cohen, "Generation of bright phase-matched circularly-polarized extreme ultraviolet high harmonics," Nat. Photonics **9**, 99–105 (2014).
48. C. Chen, Z. Tao, C. Hernández-García, P. Matyba, A. Carr, R. Knut, O. Kfir, D. Zusin, C. Gentry, P. Grychtol, O. Cohen, L. Plaja, A. Becker, A. Jaron-Becker, H. Kapteyn, and M. Murnane, "Tomographic reconstruction of circularly polarized high-harmonic fields: 3D attosecond metrology," Sci. Adv. **2**, e1501333 (2016).
49. X. Zhang, X. Zhu, X. Liu, D. Wang, Q. Zhang, P. Lan, and P. Lu, "Ellipticity-tunable attosecond XUV pulse generation with a rotating bichromatic circularly polarized laser field," Opt. Lett. **42**, 1027–1030 (2017).
50. S. A. Rezvani, Z. Hong, X. Pang, S. Wu, Q. Zhang, and P. Lu, "Ultrabroadband tunable OPA design using a spectrally broadened pump source," Opt. Lett. **42**, 3367–3370 (2017).

1. Introduction

Chiral molecules are characterized by having nonsuperposable mirror images. The two images are known as R-enantiomer and S-enantiomer, possessing a left and right handedness, respectively. The enantiomers have the same chemical and physical properties such as boiling point, melting point, density, etc, but exhibit different interactions with another chiral object. Chirality plays an important role in chemisity and medicine, but detecting and quantifying it remain challenging. The conventional chiroptical spectroscopies [1], such as the optical rotation, electronic and vibrational circular dichroism (CD), and Raman optical activity, are based on the non-dipole chiral interactions. In these techniques, the magnetic transition dipoles lead to the discrimination in spectroscopy for two enantiomers. However, the magnetic effects are weak, which resultes in weak chiral responses. This weak chiral response also poses challenges for the time-resolved measurements of chiral dynamics. To gain an insight into the dynamical mechanism of chiral response, it is necessary to develop the spectroscopic techniques with strong signals and high temporal resolution. For example, in the past decades, several methods based on the electric-dipole effects have been developed [2–4], since the electric-dipole effects are generally stronger than the conventional chiral effects.

Recently, with the fast development of laser technology, the photoelectron circular dichroism (PECD) using table-top femtosecond laser pulses was proposed [5]. In the PECD, an asymmetry in the forward-backward electron emission induced by circularly polarized (CP) laser pulses can be observed in photoelectron angular distributions [3–7]. It has been reported that chirality can be detected with high harmonic generation (HHG) lately [8–10]. HHG, resulting from the nonlinear interaction of intense laser pulses with a gas medium, has been proved to be a valuable tool for attosecond science [11]. It has been applied to the production of attosecond pulses [12–14], the observation and control of ultrafast dynamics [15–20], and the imaging of molecular orbitals [21–23].

The mechanism of HHG can be intuitively understood in terms of the three-step model [24, 25], where the HHG process consists of three steps: tunnel ionization of the outer valence electrons, acceleration of the liberated electrons induced by the intense laser pulse, and the

Optics EXPRESS

emission of high-energy photons (high-order harmonics) when the electrons return to the vicinity of the parent ions. The chiral HHG (cHHG) method has several characteristics, such as high enantio-sensitivity and subfemtosecond resolution, which makes it a powerful tool for ultrafast chiroptical detection [8, 9].

In previous works, only chiral molecules whose chiral element is chirality center (also called asymmetric carbon) are studied. However, another type of chiral element is possible. For example, axial chiral molecules, whose stereogenic element is an axis rather than a single atom, can exhibit axial stereochemistry. The enantiomers of axial chiral compounds are usually specified by the stereodescriptors R_a (right handedness) and S_a (left handedness). There are myriad natural products and biomolecules that contain axial chirality [26, 27]. Furthermore, axial chiral compounds play an important role in asymmetric catalysis and synthesis, pharmaceuticals and material science [27–30]. Revealing the ultrafast dynamics in axial chiral molecules is of great significance because it will help people clearly understand the basic processes in chiral reaction, for example, axial-to-central chirality transfer. Those dynamics could be resolved by the recently developed techniques based on the interaction with the ultrafast laser pulses [11]. However, the involved strong-field processes, such as the strong-field ionization and HHG, have never been discussed before.

In this work, HHG resulting from the interactions of axial chiral molecules with CP and bichromatic counterrotating circularly polarized (BCCP) laser pulses is studied. A typical and simple class of axial chiral compounds, called axial chiral allenes , is used as the prototype here. Axial chiral allenes contain an even number of consecutive double bonds. In contrast, we also study the HHG from propadiene (achiral molecule) with BCCP laser pulses. The CD of HHG from axial chiral and achiral molecules in both 3D and 1D orientation are discussed. The simulated results are all qualitatively explained with the trajectory analysis based on the semiclassical three-step mechanism of HHG.

2. Theoretical model

An *ab initio* calculation based on time-dependent density functional theory (TDDFT) [31] was performed to study HHG from molecules. TDDFT has been proved to be a promising tool to study HHG [32,33]. Neglecting electron spin effects, the time-dependent electron density $n(\mathbf{r}, t)$ for the closed-shell system is calculated as:

$$n(\mathbf{r}, t) = 2\sum_{i=1}^{N} |\psi_i(\mathbf{r}, t)|^2. \tag{1}$$

Here N is the number of Kohn-Sham orbitals and $\psi_i(\mathbf{r}, t)$ is the time-dependent Kohn-Sham (KS) orbitals obtained through the time-dependent KS equations (atomic units are used throughout this paper unless otherwise stated) :

$$i\frac{\partial}{\partial t}\psi_i(\mathbf{r}, t) = \left[-\frac{1}{2}\nabla^2 + v_{ext}(\mathbf{r}, t) + v_h(n; \mathbf{r}, t) + v_{xc}(n; \mathbf{r}, t) + v_l(\mathbf{r}, t)\right]\psi_i(\mathbf{r}, t). \tag{2}$$

In Eq. (2), $v_{ext}(\mathbf{r}, t)$ is the external potential described with Hartwigsen-Goedecker-Hutter (HGH) pseudopotentials [34]. The term $v_h(n; \mathbf{r}, t)$ is the time-dependent Hartree potential, describing the interaction of classical electronic charge distributions. $v_{xc}(n; \mathbf{r}, t)$ is the exchange-correlation potential, where we choose the generalized gradient approximation (GGA) proposed by Perdew, Burke& Ernzerhof [35]. $v_l(\mathbf{r}, t) = \mathbf{r} \cdot \mathbf{E}(t)$ represents the interaction of the electrons with the laser field.

The ground state of the system is obtained through the ground-state KS equations [36, 37] :

$$\left[-\frac{1}{2}\nabla^2 + v_{ext}(\mathbf{r}) + v_h(n; \mathbf{r}) + v_{xc}(n; \mathbf{r})\right]\psi_i(\mathbf{r}) = \mathcal{E}_i\psi_i(\mathbf{r}). \tag{3}$$

Optics EXPRESS

The time-dependent KS equations are propagated in time using the approximated enforced time-reversal symmetry scheme [38]. The calculation is implemented in OCTOPUS code [39]. During the propagation, the KS wave function is multiplied at each time step by a function $M(\mathbf{r})$ to avoid the unphysical reflections at the boundaries of the simulation region [39]. The harmonic spectra can be calculated from the time-dependent dipole moment $\mathbf{d}(t)$ as:

$$H(\omega) \propto \left| \int \frac{\mathrm{d}^2}{\mathrm{d}t^2} \mathbf{d}(t) e^{i\omega t}\, dt \right|^2, \tag{4}$$

where $\mathbf{d}(t)$ is given by

$$\mathbf{d}(t) = \int n(\mathbf{r}, t)\, \mathbf{r}\, d\mathbf{r}. \tag{5}$$

Here, ω is the frequency of the high harmonics.

HHG is also investigated by strong field approximation (SFA) presented by Lewenstein *et al* [40], which allows us to obtain a relatively simple evaluation of the time dependent dipole moment. The time dependent dipole moment is calculated with the integral:

$$\mathbf{d}(t) = i \int_0^t dt' \int d^3\mathbf{p}\, \mathbf{d}^*[\mathbf{p} - \mathbf{A}(t)]\, \mathbf{E}(t') \cdot \mathbf{d}[\mathbf{p} - \mathbf{A}(t')]\, e^{-iS(\mathbf{p},t,t')} + \text{c.c.} \tag{6}$$

and

$$S(\mathbf{p}, t, t') = \int_{t'}^{t} dt'' \left(\frac{[\mathbf{p} - \mathbf{A}(t'')]^2}{2} + I_p \right), \tag{7}$$

where I_p is the ionization potential of the molecule. In Eq. (6), $\mathbf{A}(t)$ is the vector potential of the electric field $\mathbf{E}(t)$ and $\mathbf{d}[\mathbf{p} - \mathbf{A}(t)]$ is the dipole matrix element of the transition from the ground state to the continuum state characterized by the electron velocity $\mathbf{v}$ ($\mathbf{v} = \mathbf{p} - \mathbf{A}(t)$). $\mathbf{p}$ is the canonical momentum. c.c. stands for complex conjugate of the first term on the right side of Eq. (6). The highest occupied molecular orbital (HOMO), obtained by an *ab initio* calculation using a 6-31G* basis set in the Gaussian software package [41], is chosen as the ground state. The transition dipole matrix element is calculated from [42]:

$$\mathbf{d}(\mathbf{v}) = \langle \mathbf{v} | \mathbf{r} | \psi_{HOMO} \rangle. \tag{8}$$

3. Results and discussions

We first study the HHG from (S_a)-3-chloropropa-1,2-dien-1-ol with CP laser pulses. Figure. 1(a) illustrates the geometery and orientation of (S_a)-3-chloropropa-1,2-dien-1-ol in Cartesian coordinates. The chiral axis is fixed along z axis. Hydroxy group (-OH) and H atom (in the left-hand site of the molecule) are on the *xoz* plane. Cl and H atom (in right-hand site of the molecule) are on the *yoz* plane. The right (+) and left (-) CP laser fields are specified by

$$\mathbf{E}_{\pm}(t) = E_0 f(t) \left[\cos(\omega t)\, \hat{\mathbf{e}}_x + \cos\left(\omega t \pm \frac{\pi}{2}\right) \hat{\mathbf{e}}_y \right], \tag{9}$$

where ω is the angular frequency corresponding to the wavelength of 632.8 nm. In Eq. (9), $\hat{\mathbf{e}}_x$ and $\hat{\mathbf{e}}_y$ are unit vectors along the x and y axes, respectively. The amplitude of the electric field E_0 corresponds to the intensity of 3×10^{14} W/cm^2. The envelope $f(t)$ has trapezoidal shape with 2-cycle rising and falling edges and 4-cycle plateau. The time-dependent electric field of right CP laser pulse $\mathbf{E}_+(t)$ is presented in Fig. 1(b).

Figure 1(c) shows the harmonic spectrum from (S_a)-3-chloropropa-1,2-dien-1-ol obtained with TDDFT. Both odd and even harmonics are found in Fig. 1(c). This can be well explained by the selection rules [33]: this molecule belongs to C_1 point group and CP laser field possesses

Optics EXPRESS

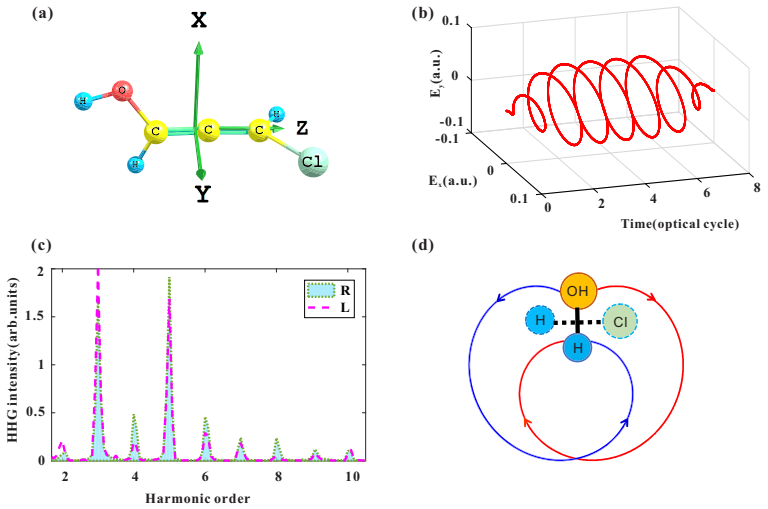

Fig. 1. (a) Geometry of (S_a)-3-chloropropa-1,2-dien-1-ol. (b) Electric field of $\mathbf{E}_+(t)$ with the intensity of 3×10^{14} W/cm^2 and wavelength of 632.8 nm. (c) HHG spectra with the right (R) and left (L) CP light. (d) Schematics of two representative electron trajectories with two oppositely polarized laser pulses. Arrows express the direction of electron motion. The blue and red curves indicate the trajectories with the right and left CP laser pulses, respectively.

C_∞ symmetry, so the allowed harmonics are $n = k \pm 1$ orders, where k is an integer. HHG spectra driven by left and right CP laser fields are different as shown in Fig. 1(c), i.e. the HHG exhibits obvious CD. To better understand the HHG process and explain the CD for axial chiral molecule with CP light, we perform a trajectory analysis based on the semiclassical three-step model [25, 43, 44]. This method has been successfully used in previous works [10]. Here we simplify the substituents (such as OH, H, and Cl) as spheres with different radius so as to show the primary factor in CD for axial chiral molecules. A $\rightarrow$ B is used to denote that the electrons tunnel from A (atom or substituents) and then return to the vicinity of B (atom, or substituents). Considering that the polarized plane of $\mathbf{E}(t)$ is parallel to xoy plane, we can predigest the molecules as two parts (OH—H and H—Cl) when we study the relationship between the electron trajectories and the CD of HHG. For the left site ($z < 0$) of (Sa)-3-chloropropa-1,2-dien-1-ol, OH $\rightarrow$ H and OH $\rightarrow$ OH are possible and the electron trajectories should be symmetrical with left and right CP light when the Coulomb potential in molecule is neglected. Here we only choose OH $\rightarrow$ H as an example. In order to have a clear picture of the electron motion, we illustrate two representative trajectories for OH $\rightarrow$ H in Fig. 1(d). One can see that, both two trajectories have the same spiral shape due to the CP driving field. However, when the Coulomb potential is taken into account, the two trajectories are asymmetrical because the effect of Coulomb potential from Cl and H in the right-hand side are different. As a result, the HHG processes in left and right CP fields are different, resulting in the CD of HHG. Basically, the CD of HHG here results from the chiral structure of the molecule that the substituents on each side must be different.

Due to the rescattering feature of HHG process, HHG driven by CP laser pulses has some problems, such as low efficiency [25, 45] and low cutoff frequencies [46]. These shortages are adverse to its possible applications, like chiral discrimination. In additions, CD from CP pulses is sensitive to the laser wavelength and length of the chiral axis. As discussed above, axial chiral molecules exhibit CD in responds to CP laser pulse because of the asymmetric Coulomb effect on the other side. If the length of chiral axis is much longer or the wavelength of the driving laser is shorter, the transverse spreading of the recolliding electron wave packet would be much

Optics EXPRESS

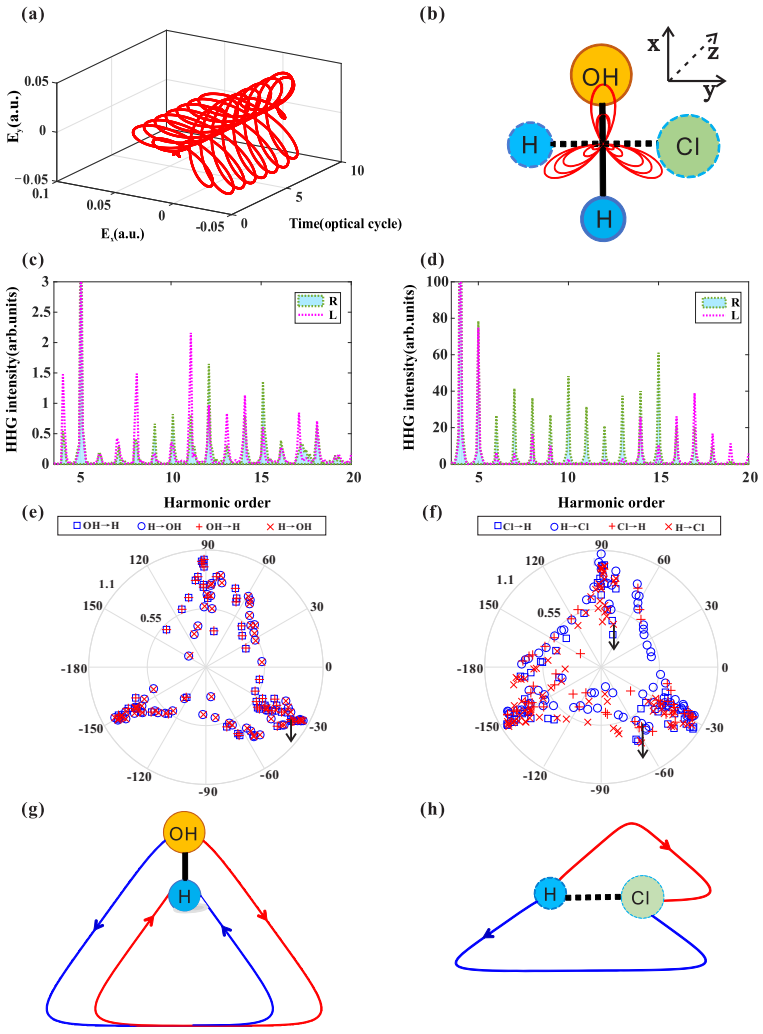

Fig. 2. (a) Electric field of $\mathbf{E}_+(t)$. (b) Projections of $\mathbf{E}_+(t)$ and the molecule on the xoy plane. (c), (d) HHG simulated by TDDFT and SFA, respectively. (e), (f) The electron momentum distributions calculated by semiclassical model. The blue and red marks are the results with $\mathbf{E}_+$ and $\mathbf{E}_-$, respectively. (g), (h) Schematics of the representative electron trajectories corresponding to the circles and squares indicated by the ↓ in (e), (f).

shorter than the length of the chiral axis. Thus the Coulomb potential from the other side would be negligible and HHG from axial chiral molecules driven by CP light might not show CD. This implies that, HHG with CP laser pulses could not be used to distinguish the chirality of the target molecule, because the CD is still sensitive to other factors.

To avoid these problems, we adopt the BCCP laser fields. HHG from atoms and simple molecules driven by the BCCP laser fields has been widely studied [47–49]. With the BCCP pulses, the HHG efficiency will be dramatically increased and the cutoff can be also extended. In the following, we will show that the CD of HHG with BCCP laser fields is determined directly by the chiral structure of the molecule, irrespective of the consideration of Coulomb potential.

The BCCP pulse is composed of a superposition of two coplanar counter-rotating CP laser

Optics EXPRESS

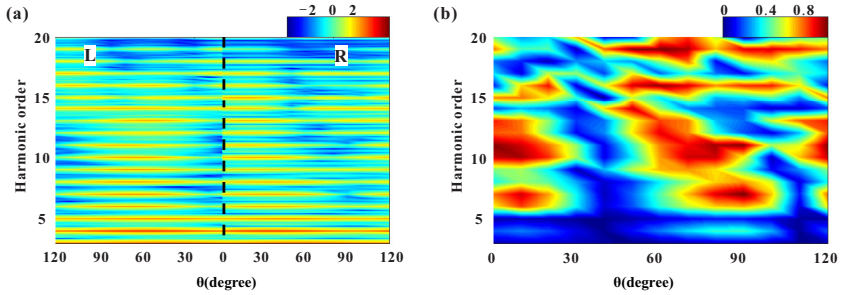

Fig. 3. (a) Logarithm of $I_R(n,\theta)$ and $I_L(n,\theta)$ from (S_a)-3-chloropropa-1,2-dien-1-ol with BCCP laser fields. (b) CD signal $\eta(n,\theta)$ obtained from (a).

pulses. The right (+) and left (-) BCCP laser pulses are specified by

$$E_{\pm}(t) = E_0 f(t) \left(E_1 \hat{\mathbf{e}}_x \pm E_2 \hat{\mathbf{e}}_y\right) \tag{10}$$

with

$$E_1 = \cos(\omega t) + \cos(2\omega t)\,,\ E_2 = \cos\left(\omega t + \frac{\pi}{2}\right) - \cos\left(2\omega t + \frac{\pi}{2}\right). \tag{11}$$

In Eq. (10), $f(t)$ is the trapezoidal envelope with 2-cycle (corresponding to the cycle of $\lambda = 1000$ nm) rising and falling edges and 6-cycle plateau. The electric field amplitude E_0 corresponds to the intensity of $I = 2.5 \times 10^{13}$ W/cm^2. In Eq. (11), the frequency ω corresponds to laser wavelengths of $\lambda = 1000$ nm [50].

Figure 2(a) shows the electric field of $\mathbf{E}_+(t)$. Figure. 2(b) shows the projections of $\mathbf{E}_+(t)$ and (S_a)-3-chloropropa-1,2-dien-1-ol on xoy plane. The total electric field vector $\mathbf{E}_+(t)$ traces out a trefoil pattern whose three lobes are separated by $2\pi/3$ in Fig. 2(b). The time-dependent electric field has three maxima per laser cycle. HHG spectra stimulated by TDDFT and SFA with the BCCP laser pulses are presented in Figs. 2(c) and 2(d). The BCCP laser field possesses threefold rotational symmetry and this axial chiral molecule belongs to C_1 point group, so both odd and even harmonic orders can be observed [33]. From Figs. 2(c) and 2(d), one can see that HHG driven by $\mathbf{E}_+(t)$ (R) and $\mathbf{E}_-(t)$ (L) is different, i.e. both the results with TDDFT and SFA show prominent CD.

To analyze the HHG process and explain the origin of the CD, in Figs. 2(e) and 2(f), we calculate the distribution of electron momentum at the moment of recollision based on semiclassical model [25]. Each point in the distribution corresponds to an electron trajectory. All the sign of the return angles with $\mathbf{E}_-$ are reversed to make the symmetry of the distributions prominent. In the analysis, we first neglect the effect of the Coulomb potential. For A → A, the electron trajectories with two oppositely BCCP laser fields are symmetrical. Therefore we just consider A → B (A is different from B). As shown in Fig. 2(e), neglecting the Coulomb potential, the electron momentum distribution of OH and H in $z < 0$ is symmetrical, but the momentum distribution in Fig. 2(f) for H and Cl in $z > 0$ is asymmetric.

To obtain a clear picture of the trajectories, we plot representative electron trajectories in Figs. 2(g) and 2(h). The corresponding recolliding moments are indicated in Figs. 2(e) and 2(f) by the arrows. For the trajectory with $\mathbf{E}_+$ shown in Fig. 2(g), the electron starts from OH, moves anticlockwise and finally returns to the H atom after it arrives to the maximal excursion in $y > 0$ area. Its trajectory (blue line) has a triangular shape that reflects the threefold symmetry of the BCCP laser fields. For the trajectory with $\mathbf{E}_-$ shown in Fig. 2(g), the electron starts from OH and move clockwise. It also possesses a triangular shape trajectory (red line) and finally recollide to H. Note that, the momentum distribution shown in Fig. 2(e) and the trajectories shown in Fig. 2(g) with $\mathbf{E}_-$ and $\mathbf{E}_+$ are symmetrical. This indicates that HHG contributed from the $z < 0$

Optics EXPRESS

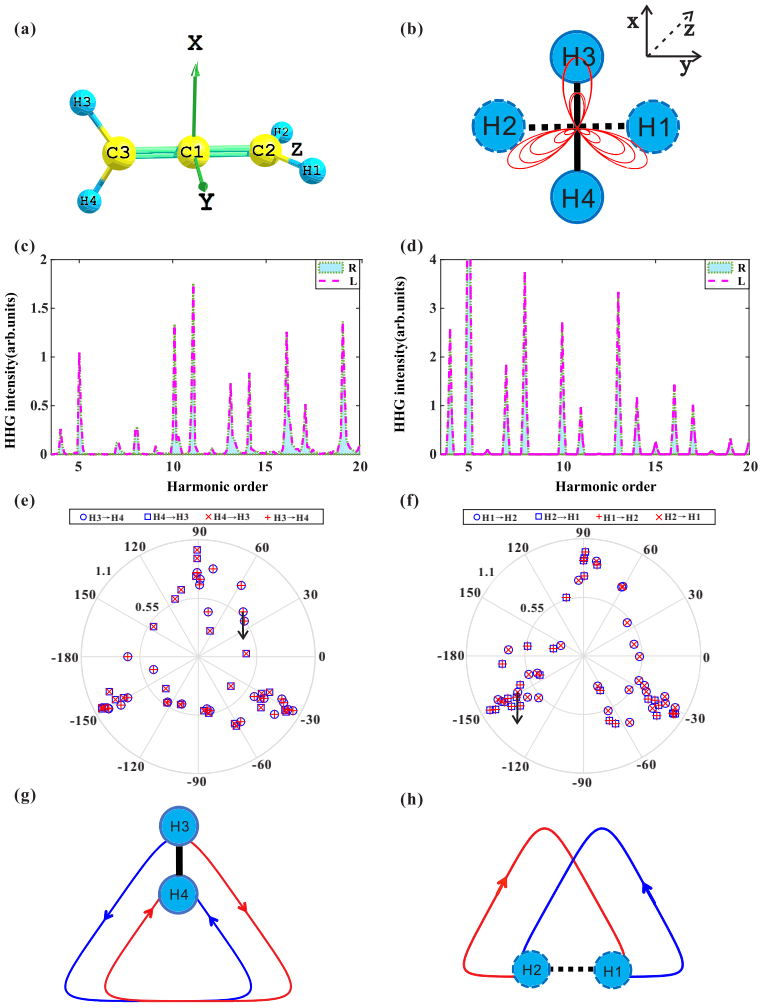

Fig. 4. (a) Geometry of propadiene. (b) Projections of $\mathbf{E}_+(0)$ and propadiene on the xoy plane. (c), (d) HHG simulated by TDDFT and SFA, respectively. (e), (f) The electron momentum distributions calculated by semiclassical model. The blue and red marks are the results with $\mathbf{E}_+$ and $\mathbf{E}_-$, respectively. All the sign of the return angles with $\mathbf{E}_-$ are reversed for comparison of the distributions. (g), (h) Schematics of the representative electron trajectories corresponding to the circles and squares indicated by the ↓ in (e), (f).

is the same in the left ($\mathbf{E}_-$) and right ($\mathbf{E}_+$) polarized fields. On the contrary, the momentum distribution and the trajectories shown in Figs. 2(f) and 2(h) are prominently asymmetrical. As a result, the HHG of the whole molecule in the $\mathbf{E}_+$ and $\mathbf{E}_-$ fields are different and obvious CD can be found.

If the BCCP laser field is rotated by an angle θ around z axis, the HHG processes in both $z < 0$ and $z > 0$ are asymmetrical in the E_+ and E_- fields (except in the case θ being an integer of $\pi/2$, where either the process in $z < 0$ or $z > 0$ must be different as was discussed above). Therefore, HHG driven by the BCCP laser fields could exhibit CD at any angle. From the discussions we can see that, the CD of HHG from the chiral molecules right originates from the chiral structure in which the substituents bonded to the chiral axis in each side must be different. The above discussions and conclusions will remain the same when the Coulomb effect

Optics EXPRESS

is then taken into account, because the effect of the Coulomb potential are also asymmetrical due to the chiral structure. The asymmetrical Coulmb effect will also result in the asymmetry of the electron trajectories and the CD of HHG.

In order to quantitate the discrimination of HHG, we define the CD signal as :

$$\eta(n,\theta) = \frac{|I_L(n,\theta) - I_R(n,\theta)|}{I_L(n,\theta) + I_R(n,\theta)}, \tag{12}$$

where $I_{R,L}(n,\theta)$ are the yields of harmonic n for right (+) and left (-) polarized BCCP laser fields. The new electric field rotated by θ is $\mathbf{E}(\theta) = \hat{R}(\theta)\mathbf{E}(0)$, where $\hat{R}(\theta)$ is the rotation matrix expressed as:

$$\hat{R}(\theta) = \begin{bmatrix} \cos\theta & -\sin\theta \\ \sin\theta & \cos\theta \end{bmatrix}. \tag{13}$$

Considering the trefoil pattern of the BCCP laser fields, we just need to discuss the CD signal with $\theta \in [0, 2\pi/3]$. Note that the HHG simulated by both TDDFT and SFA is similar and shows the same conclusion for the CD, which has been confirmed by both the calculations shown in this paper and others not shown here. Thus we calculate the harmonic spectra by SFA, as show in Fig. 3(a), in order to decrease time consumption. HHG spectra in Fig. 3(a) for (S_a)-3-chloropropa-1,2-dien-1-ol with the BCCP laser fields show clear discriminations at all angles. The dichroism is further presented in Fig. 3(b) in terms of $\eta(n,\theta)$, which is up to 0.8. This results is consistent with our discussion above.

In order to have a better understanding of the CD in axial chiral molecules, we consider an achiral molecule propadiene for comparison. As shown in Fig. 4(a), propadiene molecule has four identical H atom. For the sake of clearness in analysis, we add labels to each H atom. Figure 4(b) illustrates the geometry of the BCCP laser field and propadiene. Figures 4(c) and 4(d) show that the HHG spectra from propadiene stimulated by TDDFT and SFA have no CD. The distributions of electron momentum at the moment of recollision for propadiene are also calculated. As shown in Figs. 4(e) and 4(f), the distributions of electron recollision momentum for H3—H4 and H1—H2 with two oppositely polarized BCCP laser fields are symmetrical. The representative trajectories are shown in Figs. 4(g) and 4(h), which corresponds to the four recombination indicated by the arrows in Figs. 4(e) and 4(f). For H3 → H4, the electron trajectories are symmetrical under two oppositely polarized BCCP laser fields. For H1—H2, the trajectories of H1 → H2 with the right polarized light are symmetrical with the trajectories of H2 → H1 with the left polarized light in Fig. 4(f). This trajectory analysis can then well explain the fact that no CD is found for achiral molecules. The substituents are symmetrically distributed and then the HHG processes must be the same under laser fields with opposite rotation directions. One can obtain the same conclusion when the Coulomb potential is considered, because the Coulomb effect should be also symmetrical in the achiral structure.

HHG from propadiene and CD signal at $\theta \in [0, 2\pi/3]$ are also calculated so as to compare with (S_a)-3-chloropropa-1i,2-dien-1-ol in Figs. 5(a) and 5(b). As show in Fig. 5(b), HHG from propadiene displays no CD at any angle. In summary, HHG driven by the BCCP laser fields from axial chiral molecules has CD, but HHG from achiral molecules has no CD. The origin of CD for 3D aligned axial chiral molecules can be well understood from the fact that the trajectories (final electron momentum distributions) are asymmetric. This feature is right due to the chiral structure of the molecule and the semiclassical three-step mechanism of HHG.

Note that, since the molecules are oriented, the CD is dominantly determined by the dipole effect instead of the non-dipole chiral effect. Therefore, the theoretical models within dipole approximation are applied, where the light has only the x and y components while does not have the z component (along the propagation direction). Considering this, the CD of HHG in this work can also be explained by the symmetry of system. For the circularly polarized laser, the clockwise laser field can be transformed to the counter-clockwise laser field by a 180-

Optics EXPRESS

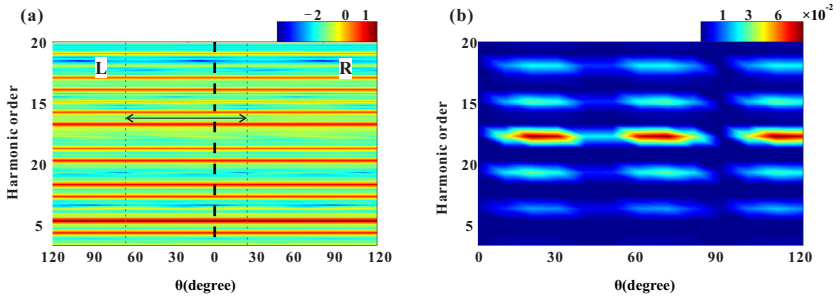

Fig. 5. (a) Logarithm of $I_R(n,\theta)$ and $I_L(n,\theta)$ from propadiene with BCCP laser fields. (b) CD signal $\eta(n,\theta)$ obtained from (a).

degree rotation around the x axis and vice versa. If the molecule (or the molecule ensemble discussed below) is symmetric with respect to this operation (i.e. has a C_2 axis along x axis) or with respect to this operation followed by a reflection about the xoy plane (for simplicity, we denote the molecule has a $\sigma_{xy}C_2$ axis along the x direction), the HHG from this molecule will be the same in left and right CP laser. On the other hand, the laser field also contains an approximate spatial-temporal symmetry, which involves a translation in time by $\Delta t = T/N$ and a simultaneous spatial rotation by $\alpha = 360/N$ degree around the z axis. $T = 2\pi/\omega$ is the periodicity of the laser and N is an arbitrary number. Combining this symmetry operation with the 180-degree rotation around the x axis, one can see that the clockwise field is approximately transformed to the counter-clockwise field by a 180-degree rotation around an axis within the xoy plane, at an angle of $\alpha/2$. Thus, if the molecule has any C_2 or $\sigma_{xy}C_2$ axis within the xoy plane, its HHG response to the left and right CP fields will be approximately the same. (They will be exactly the same is the laser pulse is infinitely long). If the molecule or ensemble does not has a C_2 or $\sigma_{xy}C_2$ axis within the xoy plane, the HHG driven by left and right CP fields would be different. Since the (S_a)-3-chloropropa-1,2-dien-1-ol molecule belongs to C_1 point group, i.e. does not have a C_2 or $\sigma_{xy}C_2$ axis. Therefore, HHG from this molecule is likely to displays CD as in Fig. 1.

The analysis for the BCCP driving field is similar, and yields similar results. For the field parameters used in the manuscript, presence of a C_2 or $\sigma_{xy}C_2$ axis along the x direction will cause the response to the clockwise and counterclockwise fields to be exactly the same. Presence of a C_2 or $\sigma_{xy}C_2$ axis at ±60 or ±120 degree from the x direction (and within the xoy plane) will make the response approximately the same etc. This well explains the results in Figs. 2 and 4. Specifically, since the propadiene shown in Fig. 4(a) has a $\sigma_{xy}C_2$ in the x direction, the HHG in left and right CP pulses are the same. Note that, a molecule which has a $\sigma_{xy}C_2$ axis in the xoy plane means that it is symmetric about a plane perpendicular to the xoy plane. For example, if the axis is along the x direction, $\sigma_{xy}C_2 = \sigma_{xz}$. For the convenience of discussion, we use the notation $\sigma_{xy}C_2$.

All the above discussions are based on 3D orientation of molecules. Experiments with 1D oriented molecules can be more easily realized than with 3D oriented molecules. So we next consider molecules that are only 1D orineted. Figures 6(a) and 6(b) show the harmonic spectra for 1D oriented (S_a)-3-chloropropa-1,2-dien-1-ol and propadiene, respectively. The dichroism is further shown by the CD signal in Fig. 6(c). The result is similar to that in the case of 3D orientation, i.e. there is also obvious dichroism for 1D oriented axially chiral molecule.

For propadiene, the pair of angles α and $\beta = \pi/2 - \alpha$ always satisfies the equation $I_L(\beta) = I_R(\alpha)$. In Fig. 5(a), two dashed lines and a double-headed arrow are used to guide the eyes, where the two dash lines indicate the two angles satisfying $I_L(\beta) = I_R(\alpha)$. As a result, the total harmonic spectra summing the contribution of all the angles must be the same, and HHG

Optics EXPRESS

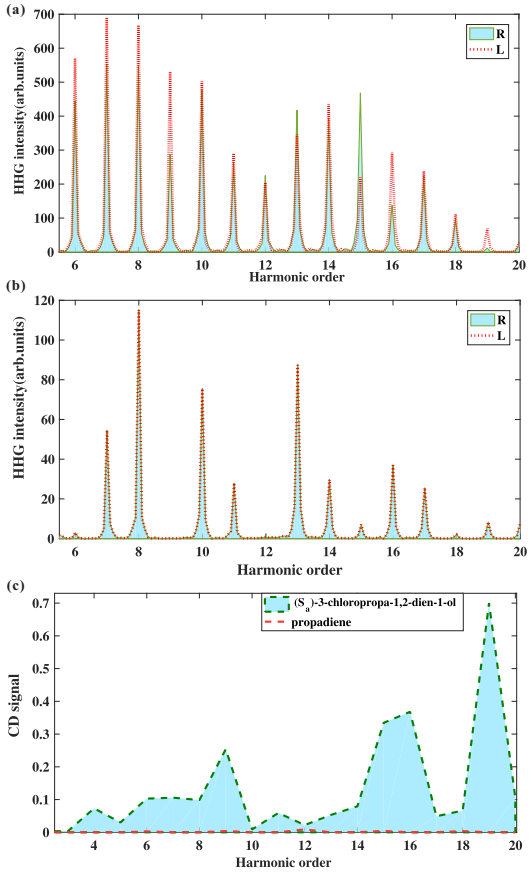

Fig. 6. (a) Harmonic spectra for 1D oriented (S_a)-3-chloropropa-1,2-dien-1-ol with BCCP laser fields. (b) Harmonic spectra for 1D oriented propadiene with BCCP laser fields. (c) CD signal for 1D oriented molecules.

from 1D oriented propadiene has no CD. This can also be proved from the Schrödinger equation. Hamiltonian of the interaction with the two oppositely polarized BCCP laser fields are

$$H_{R,L} = H_0 - \mathbf{r} \cdot \mathbf{E}_{\pm} , \tag{14}$$

where H_0 is field-free Hamiltonian. For the right BCCP light with $\theta = \alpha$, we have

$$\begin{bmatrix} E_+^{(x)}(\alpha;t) \\ E_+^{(y)}(\alpha;t) \end{bmatrix} = \hat{R}(\alpha) \begin{bmatrix} E_1(t) \\ E_2(t) \end{bmatrix} . \tag{15}$$

For the left BCCP light with $\beta = \pi/2 - \alpha$, we have

$$\begin{bmatrix} E_-^{(x)}(\beta;t) \\ E_-^{(y)}(\beta;t) \end{bmatrix} = \hat{R}(\pi/2-\alpha) \begin{bmatrix} E_1(t) \\ -E_2(t) \end{bmatrix} = \hat{R}(\alpha) \begin{bmatrix} E_2(t) \\ E_1(t) \end{bmatrix} . \tag{16}$$

In Eqs. (15) and (16), $E_{+,-}^{(x)}$ are the electric field along x direction of $\mathbf{E}_+$ and $\mathbf{E}_-$. Considering the structure of propadiene with four identical H, we have

$$H_0(x,y,z) = H_0(y,x,z) . \tag{17}$$

Optics EXPRESS

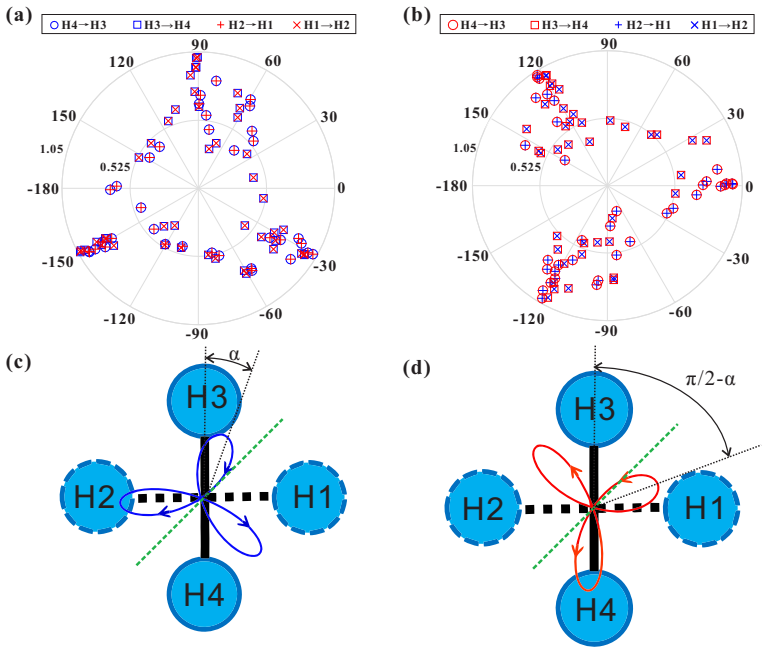

Fig. 7. (a), (b) The electron momentum distributions calculated by semiclassical model. The blue and red marks are the results with $\mathbf{E}_+$ and $\mathbf{E}_-$, respectively. (c) Schematic for the interaction between propadiene and $\mathbf{E}_+(\alpha)$. (d) Schematic for the interaction between propadiene and $\mathbf{E}_-(\pi/2-\alpha)$.

According to Eqs. (15) and (16), one can obtain

$$H_R(x,y,z,t;\alpha) = H_L(y,x,z,t;\beta). \tag{18}$$

Therefore, the wave functions in two systems satisfy

$$\psi_R(x,y,z,t;\alpha) = \psi_L(y,x,z,t;\beta). \tag{19}$$

Note that the time-dependtent dipole moment is $\mathbf{d}(t) = \langle\psi(\mathbf{r},t)|\mathbf{r}|\psi(\mathbf{r},t)\rangle$. We can derive the fowlling results

$$d_R^{(x)}(t;\alpha) = d_L^{(y)}(t;\beta), \tag{20}$$

$$d_L^{(x)}(t;\alpha) = d_R^{(y)}(t;\beta). \tag{21}$$

In Eqs. (20) and (21), $d_{L/R}^{(x/y)}(t)$ denote the time-dependent dipole momentum along x/y direction with left/right BCCP laser fields. Combining Eqs. (20), (21) and (4), one can conclude that $I_L(\pi/2-\alpha) = I_R(\alpha)$. Thus for 1D oriented propadiene, HHG still does not show CD. The equation $I_L(\pi/2-\alpha) = I_R(\alpha)$ can also be understood based on the symmetry to the rotation operation as discussed above. As in Fig. 7, the line $y = x$ in the xoy plane is one C_2 axis of the molecule, and the system shown in Panel (d) (in $\mathbf{E}_-$) is right coincident with the 180-degree rotation of the system in Panel (c) (in $\mathbf{E}_+$) around this C_2 axis.

The classical electron trajectories can also be applied to verify the equation $I_R(\alpha) = I_L(\pi/2-\alpha)$. Figures 7(a) and 7(b) show the distributions of the recolliding momentum corresponding to the trajectories A→B. Here the recollision angle is defined as the angle between the recolliding momentum and the A→B axis. As show in Fig. 7(a), the electron momentum

Optics EXPRESS

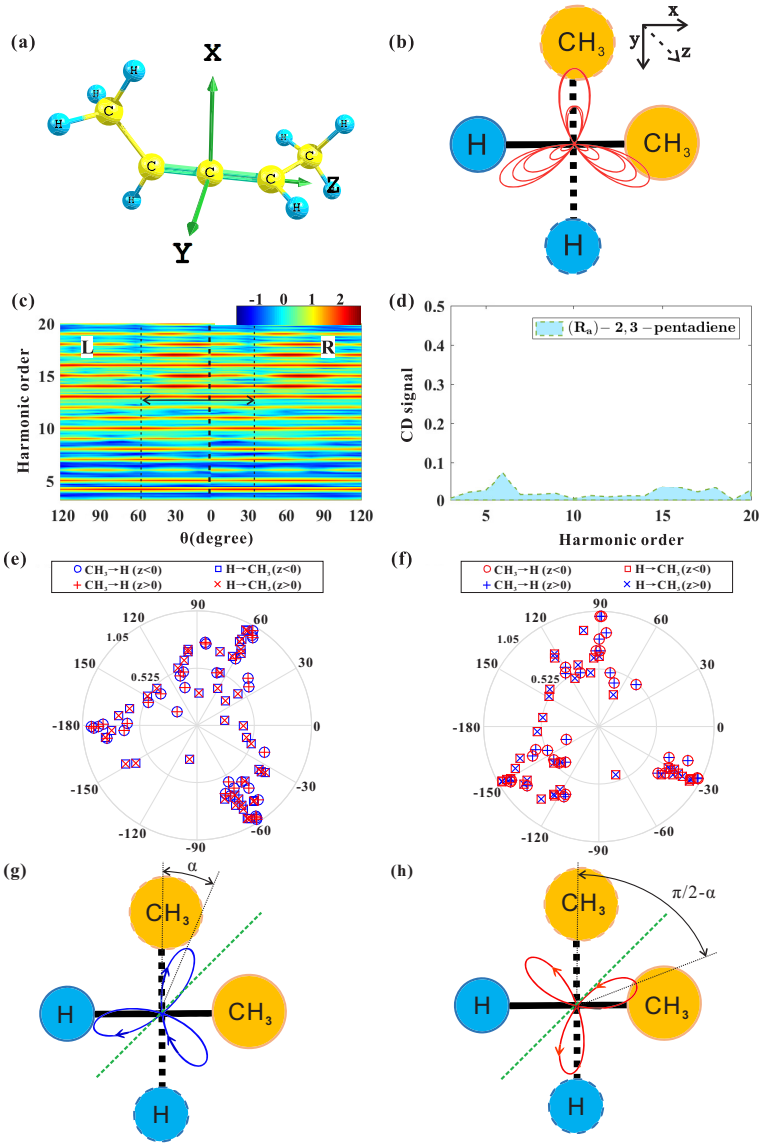

Fig. 8. (a) Geometry of (R_a)-2,3-pentadiene. (b) Projections of (R_a)-2,3-pentadiene and $\mathbf{E}'(0)$ on the xoy plane. (c) HHG spectra simulated by SFA. (d) CD signal for 1D oriented (R_a)-2,3-pentadiene. (e), (f) The electron momentum distributions calculated by semiclassical model. The blue and red marks are results with $\mathbf{E}_+$ and $\mathbf{E}_-$, respectively. All the sign of the return angles with $\mathbf{E}_-$ are reversed for comparison of the distributions. (g) Schematic for the interaction between (R_a)-2,3-pentadiene and $\mathbf{E}_+(\alpha)$. (h) Schematic for the interaction between (R_a)-2,3-pentadiene and $\mathbf{E}_-(\pi/2-\alpha)$

distributions for H4 → H3 (and H3 → H4) with $\mathbf{E}_+(\alpha)$ ($\alpha = 0$) and H2 → H1 (and H1 → H2) with $\mathbf{E}_-(\pi/2-\alpha)$ are identical. In Fig. 7(b), The distributions for H1 → H2 (and H2 → H1) with $\mathbf{E}_+(\alpha)$ are identical to the distribution for H2 → H1 (and H1 → H2) with $\mathbf{E}_-(\pi/2-\alpha)$. This can be more intuitively understood from Figs. 7(c) and (d). One can see that, the HHG processes in the laser fields $\hat{R}(\alpha)\mathbf{E}_+$ and $\hat{R}(\beta = \pi/2-\alpha)\mathbf{E}_-$ are symmetrical about the line, which divides the first and third quadrant equally (shown by the green dashed line) for any angle α. This well

explains the fact that the electron momentum distributions with $\mathbf{E}_+(\alpha)$ and $\mathbf{E}_-(\pi/2-\alpha)$ are identical and the harmonic emission $I_R(\alpha) = I_L(\pi/2-\alpha)$.

There is a special kind of axial chiral molecules which has the structure: abC=C=Cab (a,b are different substituents). This kind of axial chiral molecules belongs to C_2 point group. Here 2,3-pentadiene is chosen as a representative to study HHG from this kind of axial chiral molecules. Figure 8(a) shows the geometry and orientation of (R_a)-2,3-pentadiene. The electric-field vector $\mathbf{E}'_+(t)$ and the molecule are shown in Fig. 8(b). Harmonic spectra with left and right BCCP laser fields are presented in Fig. 8(c). It is shown that the HHG of 3D oriented (R_a)-2,3-pentadiene has notable CD at all angles except 45 degree. This is because the molecule has only one C_2 axis at 45 degree. This result is the same as that for (S_a)-3-chloropropa-1,2-dien-1-ol. However, the molecule has a C_2 axis in xoy plane and therefore the intensity of HHG is the same in $\hat{R}(\alpha)\mathbf{E}_+$ and $\hat{R}(\beta=\pi/2-\alpha)\mathbf{E}_-$ laser fields as was shown in Fig. 8(c). Two dashed lines and a double-headed arrow are used to guide the eyes, where the two dashed lines indicate the two angles satisfying $I_L(\beta) = I_R(\alpha)$. Therefore, as a chiral molecules, HHG from this special kind of molecule belonging to C_2 point group has no CD in 1D orientation as shown in Fig. 8(d).

Similarly, this phenomenon can be explained from the Hamiltonian. For (R_a)-2,3-pentadiene, one can know

$$H_0(x,y,z) = H_0(-y,-x,-z)\,. \tag{22}$$

Thus Eqs. (20) and (21) can also be derived for (R_a)-2,3-pentadiene, which means that HHG driven by left and right polarized BCCP light are identical for 1D oriented (R_a)-2,3-pentadiene. This phenomenon can also be explained by the electron trajectories based on the three-step model. Here we consider the CH_3 substituent as a sphere and calculate the electron momentum distributions when the electron return the vicinity of the partient molecule ions under $\mathbf{E}'_+(\alpha)$ and $\mathbf{E}'_-(\pi/2-\alpha)$. As shown in Figs. 8(e) and 8(f), the electron momentum distributions with $\mathbf{E}'_+(\alpha)$ and $\mathbf{E}'_-(\pi/2-\alpha)$ at the moment of recollision are identical. The symmetry of the recolliding momentum distributions can be intuitively understood from Figs. 8(g) and 8(h), which show the projections of (R_a)-2,3-pentadiene with $\mathbf{E}'_+(\alpha)$ and $\mathbf{E}'_-(\pi/2-\alpha)$ respectively. One can see that the HHG process in $\mathbf{E}'_+(\alpha)$ is symmetrical to that in $\mathbf{E}'_-(\pi/2-\alpha)$.

4. Conclusion

In this work, we have studied HHG from axial chiral molecules with BCCP laser fields. It is shown that the HHG spectra from 3D oriented molecules shows distinct chiral discriminations. Moreover, the CD can still be found when the axial chiral molecules like (S_a) -3-chloropropa-1,2-dien-1-ol are in 1D orientation. In addition, for a special kind of axial chiral molecules belonging to C_2 point group, there is no CD in HHG when the molecules are only 1D oriented. The correspondence between the HHG discriminations and the electron trajectories is discussed based on the semiclassical model. With the trajectory analysis, we can give a clear interpretation of the CD of HHG from axial chiral molecules. Our method could be applied to more complex axial chiral molecules, and all the studies would provide insights into the ultrafast chiral dynamics in the widespread axial chiral molecules like biomolecules and pharmaceuticals.

Funding

National Natural Science Foundation of China (NSFC) (11234004, 11404123, 11574101, 11422435, 11627809).

Acknowledgments

Numerical simulations presented in this paper were carried out using the High Performance Computing Center experimental testbed in SCTS/CGCL (see http://grid.hust.edu.cn/hpcc).